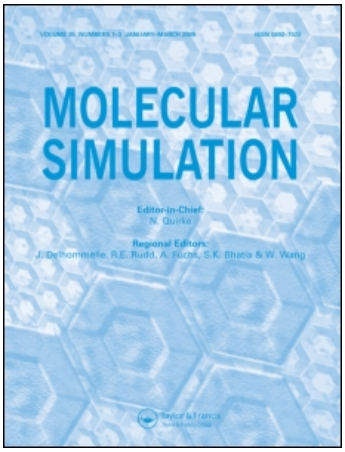

Molecular Simulation
Publication details, including instructions for authors and subscription information:
http://www.informaworld.com/smpp/title~content=t713644482

On the Role of Density Fluctuations in the Equation of State of a Simple Fluid

Jan Westergren[a]; Sture Nordholm[a]; Robert Penfold[b]
[a] Department of Physcial Chemistry, GÖteborg University, GÖteborg, Sweden [b] Institute of Food Research, Norwich, UK

To cite this Article Westergren, Jan , Nordholm, Sture and Penfold, Robert(2001) 'On the Role of Density Fluctuations in the Equation of State of a Simple Fluid', Molecular Simulation, 27: 1, 17 — 41
To link to this Article: DOI: 10.1080/08927020108024517
URL: http://dx.doi.org/10.1080/08927020108024517

Molecular Simulation, 2001, Vol. 27, pp. 17–41
Reprints available directly from the publisher
Photocopying permitted by license only

ON THE ROLE OF DENSITY FLUCTUATIONS IN THE EQUATION OF STATE OF A SIMPLE FLUID

JAN WESTERGREN[a], STURE NORDHOLM[a] and ROBERT PENFOLD[b,*]

[a]*Department of Physical Chemistry, Göteborg University, SE-412 96 Göteborg, Sweden;* [b]*Institute of Food Research, Norwich Research Park, Colney, Norwich, NR4 7UA, UK*

(Received September 2000; accepted October 2000)

We address the wellknown problems introduced into the theory of fluids by density fluctuations in the form of van der Waals loops and nonclassical critical phenomena. A clean separation of long and short range density fluctuations is achieved by use of cell-constrained models which display well-defined van der Waals loops and classical behaviour around the critical point. For a pure Lennard-Jones fluid with occupancy restricted to 1 or 8 particles per cell, the phase diagram is determined by Monte Carlo simulation. By considering the deviations from the normal simulations without cell constraint, the effects of longer range density fluctuations are exposed. The system size dependence of the van der Waals loops present in all simulations of fluids is analyzed in terms of the GvdW free energy density functional theory, which is formulated on the basis of the cell concept. The loops are found to gradually disappear either with greater cell occupancy or increasing total particle number in the simulation box.

Keywords: Cell models; Phase diagrams; Van der Waals loops

INTRODUCTION

The study of fluids has been revolutionized by the growing ability to simulate the microscopic structures and interactions which bring about the macroscopically observable properties. Most prominent of all the properties of a fluid is its equation of state, *i.e.*, the pressure as a function of temperature and density (or volume). Unfortunately, the phase transition

*Corresponding author.

between liquid and gas and the concomitant density fluctuations which arise in a two-phase coexistence region of the phase diagram is a severe problem for the Monte Carlo or molecular dynamics (MD) simulation methods now applied to fluids [1, 2]. The reason is that the fluctuations are enhanced by bubble or drop formation while the growth and decay of these structures occur on a slower timescale than ordinary single phase fluid fluctuations [3]. Thus, the generation of a complete equation of state for a fluid with the normal phase diagram exhibiting gas–liquid condensation is far from routine. Interestingly, the equations of state used in practice show little overt indication of the fluctuations where the coexistence boundary is determined by the Maxwell construction, a thermodynamic consistency argument of rather more purely mathematical character. The original form of the equation of state actually refers to a uniform fluid where the possibility of phase separation and large scale fluctuations has been eliminated. Exactly how such fluctuations are damped out is hardly ever discussed in the context of equations of state.

The presence of density fluctuations with their sometimes dramatic effects has been known for a long time [4]. Special methods have been developed to study the nonclassical fluctuations around the critical point. It would appear natural to seek equations of state which incorporate long range density fluctuations correctly. Progress in this direction has, however, been hindered by the considerable complexity encountered over the full spectrum of fluid behaviour. In this work we shall explore a different approach to the problem which we believe will eventually provide a very practical solution. Fluid models are proposed which clearly eliminate long range density fluctuations by confining the particles to cells of specified occupancy. This may seem at first to merely exacerbate the error, but there will be at least three important advantages:

(1) the error will be of a clear and precise form associated with long range density fluctuations;
(2) the simulation of such cell-constrained fluids will be much simplified by the absence of convergence difficulties associated with phase separations and critical fluctuations;
(3) a generic basis for the effects arising from long range density fluctuations permits the error to be analyzed and estimated by general methods.

We suggest that these advantages will be of considerable practical benefit. The error can be assessed in relation to the application. It can be reduced, if not eliminated, by increase of system size. Simulations can be applied more readily by routine procedures which do not require *a priori* information

about the phase diagram. The convergence should be fast enough that simulation results can become definitive for given system size and reproducible by different simulators with various codes. In the longer term, the most important advantage may be that the error is *generic*, *i.e.*, either independent or only weakly dependent on the detailed molecular model defining the fluid. Thus the error analysis is systematic and general for all fluids. It is anticipated that the renormalization group approach and other methods of a similar nature will eventually allow the predictions of a cell-constrained simulation to be corrected for long range density fluctuations.

In the present work, the magnitude of the finite size error of a cell-constrained Lennard-Jones fluid is investigated by comparing results for 1 or 8 particles per cell with corresponding results for the standard models with periodic boundary conditions imposed on boxes containing 512 particles or more. The results will be obtained in the form of state points in the (P, v)-phase diagram. To interpret these results, a few simple equations of state are developed which without being able to reproduce all details, still capture the gross features quite well. In particular, the critical properties are considered as a measure of the effect of density fluctuations in a region of greatest influence.

The debate concerning the appearance of van der Waals loops in simulations is also addressed. Although such loops are present and well converged in the cell-constrained simulations, it is not clear whether they are observable in standard periodic boundary simulations with large numbers of particles. This question was recently considered by Nakanishi and coworkers [5]. Here a density functional theory, the generalised van der Waals (GvdW) theory, is utilised in an attempt to resolve the issue. In fact, the formulation of GvdW theory draws on cell structure arguments. It therefore relates directly to the cell-constrained fluid models and allows an analysis of density fluctuations to be carried out. Thus, the relative probabilities of uniform and two-phase coexistent configurations arising in the simulation box of a normal MC or MD simulation can be estimated. As the total particle number N in the box grows, the stable configuration passes from uniform towards Maxwell reconstructed form for an interval of volume which approaches the full coexistence region as N goes to infinity. Whenever a two-phase configuration is stable, great difficulty can be anticipated in converging the simulation on starting from a uniform fluid configuration. Between the uniform initial state and the stable equilibrium configuration there is then likely to be a free energy barrier which will slow down the equilibration beyond the time scale accessible to the simulation.

CELL CONSTRAINED SIMULATION METHOD

The Monte Carlo (MC) cell simulation method used here differs from standard Metropolis scheme only by imposing an inner lattice structure subdividing the usual "global box" into "n-particle cells". Given the total number of simulated particles N with uniform cell occupancy n, the number of such cells is just $N_{\text{cell}} = N/n$. Each cell maintains its initial n particles throughout the entire simulation since trial moves which take any particle out of its cell are assigned zero probability and simply rejected. Only pure fluids are considered here, so that all particles are identical in every respect other than their positions (momenta are not sampled). In this case, the discrepancy compared to a conventional simulation can be readily assigned to the suppression of all configurations where at least two occupation numbers differ from n. This constraint damps out density fluctuations in the sampled ensemble in a well-defined manner. As the wavelength of a representable density fluctuation increases, the restriction on its amplitude becomes more severe. It is precisely the longest lived fluctuations, in terms of either real time in MD simulations or number of steps in the Markov chain for MC simulations, which are most suppressed. The result is, we claim, an optimized convergence of the simulation. As usual in an MC simulation, the type of cell structure needs to be specified (simple cubic structure will be used below) as well as an initial configuration. The Markov chain is generated by the usual Metropolis prescription with the only variation that moves altering the occupancy of any cell are rejected. The procedure also seems ideally suited for routine use in the study of bulk molecular fluids.

Of course, the validity of results obtained in such an apparently strongly constrained ensemble must be questioned. No doubt quantitative and, in some cases, qualitative differences will arise in comparison with the unconstrained fluid. Best known are the "classical" critical properties imposed by the cell structure [4, 6]. The amplitude of density fluctuations diverge at the critical point which cannot be reproduced in a cell simulation. This singular behaviour results in a shallower bowl for the coexistence curve, compared with the classical prediction, and a lower critical temperature which must therefore be overestimated in the cell simulation. Obviously, the error is most noticeable for single occupancy cell theory but even for conventional fluid simulations with hundreds or thousands of particles in the global box the problem is still persists [5]. It is also clear that any tendency towards association clustering or molecule formation in the real fluid may also increase the quantitative difference compared with experiment.

To help motivate the cell constraint, observe that the neglected communal entropy is independent of the volume for an ideal gas. Thus, the cell constrained ideal gas obeys the usual ideal gas law exactly. This is also true for a one-dimensional fluid of hard rods. Although suggestive, there is no direct evidence that a similar result also holds for realistic three-dimensional fluids. Intuitively one might suppose that dense fluids are better represented by a cell simulation than low density fluids since there would seem to be little scope for density fluctuations in the former. Over the broad class of molecular fluids, however, the true behaviour remains poorly understood. For bulk fluids, at least, it is clear that the cell constrained simulation is no less well-defined than the original unconstrained MC method. Moreover, there is every reason to believe that it will offer rapid convergence by virtue of the necessarily localized particle motion. The effects of density fluctuations can be probed systematically by increasing both cell size and particle occupation number. The most significant effects of the density fluctuations thus recovered would appear in the vicinity of the critical point. As shown below, the shifts in the critical parameters themselves, owing to the cell constraint, are about 15% for the Lennard-Jones fluid with single occupancy. By recalling the known universal scaling laws [4] for the behaviour of thermophysical properties on approaching the critical point, it should be possible to anticipate appropriate corrections without the need for an extensive series of simulations at higher occupancy.

THE PHASE DIAGRAM OF THE SINGLE PARTICLE PER CELL FLUID

Cell MC simulations have been carried out for the Lennard-Jones (12-6)(LJ) fluid with single particle occupancy over the following grid of phase points:

$v^* = v/\sigma^3 = 1.20, 1.40, 1.60, 1.75, 2.00, 2.25, 2.50, 2.75, 3.00, 3.50, 5.00$
$T^* = k_B T/\varepsilon = 0.7, 0.9, 1.1, 1.3, 1.4, 1.5, 1.6, 1.7, 2.0$ (Grid A)

These 99 phase points cover a wide region around the critical point. Reduced units are used here for volume per particle v and absolute temperature T where σ and ε are the length and energy scales, respectively, of the spherically symmetric LJ potential,

$$\phi(r) = 4\varepsilon\left((\sigma/r)^{12} - (\sigma/r)^6\right). \quad (1)$$

A space filling simple cubic cell structure is simulated with 512 particles in the global box which is repeated in space subject to the usual periodic boundary conditions. The particles are initially arranged on a regular lattice which is "melted" over a sequence of MC steps without accumulating any statistics. During the meltdown period (10^6 attempted moves), the maximal particle displacement is adjusted so that close to half the total number of trial moves are rejected. Production runs accumulated statistics over 10^7 trial moves and showed rapid convergence.

The pressure was calculated from the ensemble average of the configurational virial energy. Following convention, the potential and the virial energy are truncated at $r_c = 2.62\sigma$ and a tail correction ΔP subsequently applied so that,

$$P = P_{\text{sim}} + \Delta P, \tag{2}$$

where,

$$P_{\text{sim}} = \frac{k_B T}{v} - \frac{2\pi}{3v^2} \int_0^{r_c} dr\, r^3 g(r) \frac{d}{dr} \phi(r), \tag{3}$$

$$\Delta P = -\frac{2\pi}{3v^2} \int_{r_c}^{\infty} dr\, r^3 g(r) \frac{d}{dr} \phi(r). \tag{4}$$

Given the side length of the global cubic box L, the radial distribution function $g(r)$ is sampled for $0 \leqslant r \leqslant L/2$ and used in (4) to calculate the integral on the range $r_c \leqslant r \leqslant L/2$. For $r \geqslant L/2$, the mean field approximation is invoked (*i.e.*, $g(r) = 1$) to evaluate the remaining integral analytically. Note that the virial integral in (4) is extended over the full LJ potential (1), while $g(r)$ is obtained for the truncated potential.

Configurational correlation lengths along the Markov chain have been estimated by the method of block averages [1] and subsequently used, together with the standard deviations of the sample averages, to determine errors on the thermodynamic properties. For example, the correlation length at the phase point $T^* = 1.1$, $v^* = 2$ was obtained from the asymptotic values in Figure 1. The dashed line represents a conventional simulation where the particles were free to move out of their cells and clearly indicates much longer correlation lengths than the corresponding single occupancy cell constrained result where the relative errors in the pressure are better than 1%. As anticipated, the cell constraint effectively eliminates the convergence difficulties associated with condensation. Figure 2 illustrates the convergence in the pressure for a typical case ($T^* = 1.1$, $v^* = 2$) within

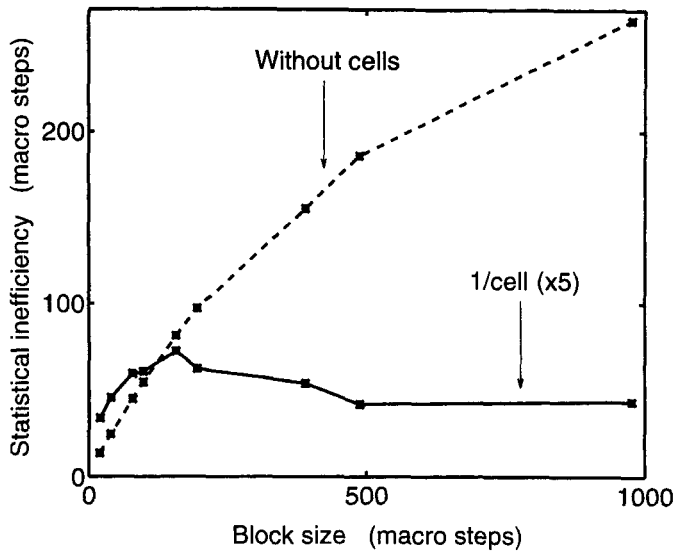

FIGURE 1 At a reduced temperature $T^* = 1.1$ and reduced volume per particle $v^* = 2.0$, the statistical inefficiency [1] is compared between a conventional global box simulation and a cell constrained algorithm with single particle occupancy per cell. A macrostep corresponds to 512 trial moves, one for each of the particles simulated. For clarity, the cell confined result has been magnified by a factor of five. Configurational correlation lengths are defined by the asymptotic values of the statistical inefficiencies. Evidently, the conventional simulation correlation length is not well determined from these results, but most probably exceeds 200 macrosteps, that is more than twenty times larger than for the cell constrained algorithm.

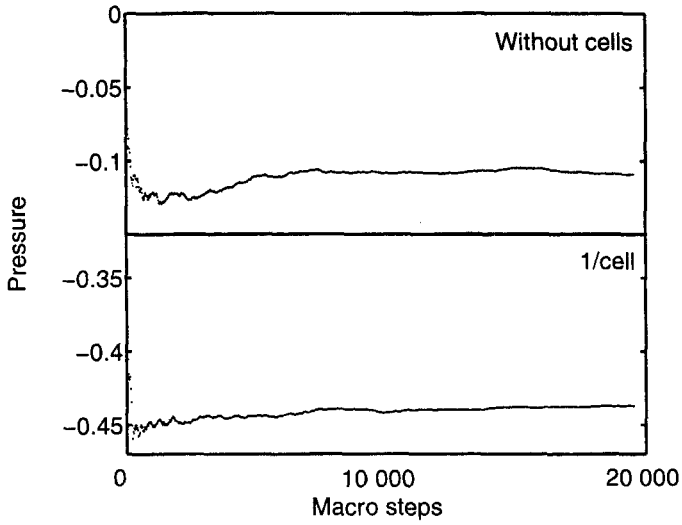

FIGURE 2 The convergence of reduced pressure as a function of Markov chain length (including meltdown) is shown for the simulations described in Figure 1.

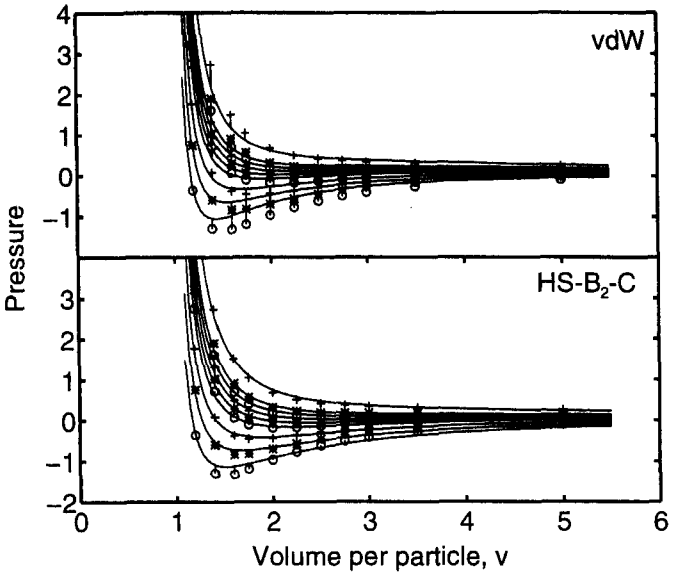

FIGURE 3 Best fit isotherms to the 99 state points (Grid A) obtained from a cell constrained simulation with single particle occupancy per cell. In all cases the statistical error, corrected for configurational correlations, is in the range $10^{-3}-10^{-2}$ in reduced pressure, so errorbars would be indiscernable on the scale of the plot. Upper panel: van der Waals equation of state. Lower panel: HS-B_2-C model.

the coexistence curve from an MC simulation both with and without the cell constraint. The conventional unconstrained simulation exhibits much slower convergence.

Pressure P as a function of volume per particle v and temperature T is the main simulation output and provides a representation of the phase diagram of the fluid over the 99 state points indicated in Figure 3. To more readily interpret this information, three simple equations of state (EOS), cubic in v, have been defined to fit the data and extract estimates of the critical properties:

(1) the van der Waals (vdW) equation of state,

$$P = \frac{k_B T}{v - b} - \frac{a}{v^2}; \tag{5}$$

(2) the GvdW(HS-B_2) equation of state,

$$P = \frac{k_B T}{v - b} - \frac{a - c k_B T}{v^2}; \tag{6}$$

(3) the GvdW(HS-B_2-C) equation of state,

$$P = \frac{k_B T}{v - b} - \frac{a - c k_B T}{(v + g)^2}. \tag{7}$$

Note that the number of parameters grows from two to four within this EOS sequence. Certainly the most celebrated, Eq. (5) needs no further comment, while the second stems from a low density hard sphere second virial coefficient correction to the bulk GvdW EOS which has been successfully used in earlier work [7]. Equation (7) is a hybrid of the GvdW(HS-B_2) result and an EOS originally proposed by Clausius [8] and more recently promoted by Martin [9], Joffe [10] and Kubic [11]. The best fit parameters were obtained by nonlinear Levenberg-Marquardt minimization [12] of the sum of squared residuals Q between simulation pressures and EOS models,

$$Q(a, b, \ldots) = \frac{1}{2} \sum_{i=1}^{99} \left(P_i^{\mathrm{MC}} - P_i(a, b, \ldots)\right)^2. \tag{8}$$

Fits were also obtained based on dispersion weighted deviations,

$$Q_w(a, b, \ldots) = \frac{\min(\xi_i^2)}{2} \sum_{i=1}^{99} \left(P_i^{\mathrm{MC}} - P_i(a, b, \ldots)\right)^2 / \xi_i^2, \tag{9}$$

where ξ_i, the standard deviation, is a measure of the uncertainty in the simulation pressure at state point i.

In all cases the minimization yielded well determined parameters of physically reasonable magnitude. From theoretical considerations, the van der Waals and GvdW(HS-B_2) EOS are commonly used with *a priori* parameters a, b and c expressed in terms of microscopic quantities defining the interaction potential. The parameter g of Eq. (7) is expected to be positive and a fraction of σ^3. Optimal parameter values together with the corresponding original GvdW values are compared in Table I. Note that the minimal Q and Q_w both decrease as the model degrees of freedom increase. It is evident from the fits shown in Figure 3 that although all three functional forms capture the essence of the data, many details of the isotherms are not well reproduced in the original van der Waals EOS. A significant improvement in the fit can be obtained, however, with the GvdW(HS-B_2) and GvdW (HS-B_2-C) equations of state.

To further appreciate the consequences of the shifts in parameter values determined here, the corresponding critical parameters implied by each EOS

TABLE I Minimized deviation, equation of state parameters and critical properties for the 99 phase points of grid A from a single particle occupancy cell constrained simulation. For each EOS. *a priori* (*ap*), weighted (*w*) and unweighted results are included

EOS	Q *or* $Q_w/99$	a	b	c	g	P_c^*	v_c^*	T_c^*	Z_c^*
vdW(*ap*)		5.585	1			0.207	3	1.65	0.375
vdW(*w*)	$1.05E-04$	6.205	1.022			0.220	3.067	1.798	0.375
vdW	$1.34E-02$	5.487	1.000			0.203	2.999	1.626	0.375
HS-B_2(*ap*)		5.585	1	1.094		0.156	3	1.25	0.375
HS-B_2(*w*)	$6.62E-05$	7.117	1.018	0.737		0.209	3.054	1.706	0.375
HS-B_2	$1.10E-02$	6.183	0.996	0.585		0.197	2.987	1.567	0.375
HS-B_2-C(*ap*)		5.585	1	1.094	0.414	0.084	3.83	0.95	0.338
HS-B_2-C(*w*)	$2.79E-05$	8.405	0.995	0.997	0.205	0.173	3.395	1.665	0.354
HS-B_2-C	$2.69E-03$	12.294	0.966	2.165	0.598	0.132	4.093	1.652	0.327

TABLE II Analytical results for the critical properties of the van der Waals, the GvdW(HS-B_2) and the GvdW(HS-B_2-C) equations of state. Note that $d=b+g$

EOS	P_c^*	v_c^*	T_c^*	Z_c^*
vdW	$a/27b^2$	$3b$	$8a/27b$	3/8
HS-B_2	$a/(27b^2+8bc)$	$3b$	$8a/(27b+8c)$	3/8
HS-B_2-C	$a/(27d^2+8dc)$	$3b+2g$	$8a/(27d+8c)$	$(3b+2g)/8d$

are also considered. For all of the EOS forms above, analytic critical properties are readily obtained from the condition,

$$\left.\frac{\partial P}{\partial v}\right|_{v=v_c} = \left.\frac{\partial^2 P}{\partial v^2}\right|_{v=v_c} = 0, \tag{10}$$

and are reported in Table II.

DETERMINATION OF THE CRITICAL POINT

The critical point is perhaps the most natural property to consider for a comparison of the phase diagrams from simulations with and without cells. Since the EOS fits on the complete data set of grid A also include many state points remote from the coexistence region, however, the critical properties quoted in Table I may more reflect the lack of model sophistication rather than describing the classical asymptotics. Therefore, a reduced subset of grid A comprising only 12 phase points and focusing on the near critical region has been identified:

$$\begin{aligned} v^* &= 2.50,\ 2.75,\ 3.00,\ 3.50 \\ T^* &= 1.6,\ 1.7,\ 2.0 \end{aligned} \qquad \text{(Grid B)}$$

Grid B has also been used to explore the cases of 8 particle cell occupancy and conventional 512 particle global box simulations without internal constraints. Pressure results on grid B have been fitted to the GvdW(HS-B_2-C) EOS model with the optimal parameters and consequent critical properties listed in Table III. Best fit isotherms are plotted in Figure 4 together with the raw data for the cases of (i) single cell occupancy, (ii) 8 particle occupancy and (iii) no cell constraints. The large symbols in Figure 4 indicate the critical points from Table III, confirming that grid B actually spans the asymptotic region while generally remaining in single phase states. Both GvdW models overestimate the critical temperature and pressure by some 20–30% while the critical volume is within about 5% of the standard

TABLE III Minimized deviation, equation of state parameters and critical properties for the 12 phase points of grid B from cell constrained simulations with either single particle ($n=1$) or 8 particle ($n=8$) occupancy per cell. Results from conventional global box simulations ($n=512$), under periodic boundary conditions, carried out in this work are also included and compared with recognised literature values [18, 19]. Excepting the compressibility factor Z_c^* the critical properties from the cell constrained simulations clearly tend towards the currently accepted values [19] upon relaxation of the occupancy restrictions. Experimental data for argon, correlated by the "best-fit" Lennard-Jones potential, are also listed

EOS	n	$Q \times 10^7/12$	a	b	c	$g \times 100$	P_c^*	v_c^*	T_c^*	Z_c^*
HS-B_2-C	1	3.78	6.790	1.168	0.075	−2.387	0.188	3.457	1.724	0.378
HS-B_2-C	8	6.81	6.418	1.073	0.835	0.9295	0.165	3.236	1.430	0.374
HS-B_2-C	512	5.14	6.243	1.106	0.854	−0.5232	0.155	3.307	1.366	0.376
LJ, Sim							0.13	3.3	1.32	0.32
Ar, Exp							0.116	3.16	1.26	0.291

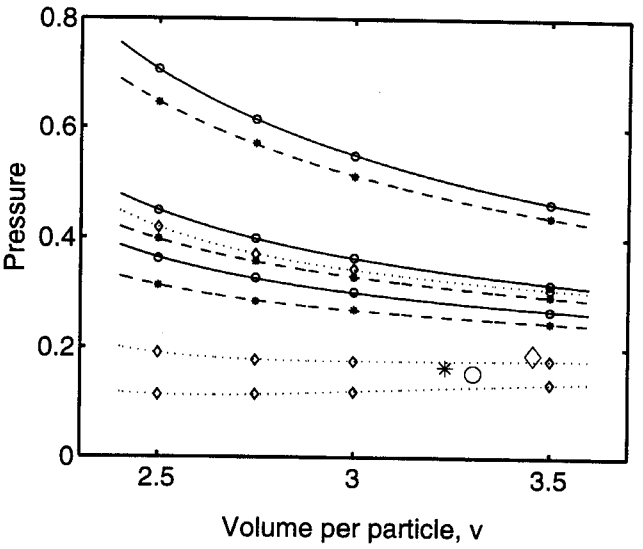

FIGURE 4 Best fit isotherms to the 12 state points (Grid B) obtained from a cell constrained simulation with single particle (···◇···) and 8 particle (– –∗– –) occupancy per cell, using the HS-B_2-C model. For comparison, an equivalent fit to conventional simulation data with no cells (—○—) is also included. The large symbols (◇, ○, ∗) indicate the corresponding critical points obtained analytically from the equation of state.

Monte Carlo result. Part of this deviation can be ascribed to physical phenomena, that is the "classical" description of critical fluctuations necessarily accompanying the cell constraints, while a purely mathematical contribution arises from the misfit of the simulation results afforded by the crude GvdW equations of state.

Although the fit appears excellent to casual observation, the predicted critical properties are rather sensitive to the selection of data. Moreover, the choice of EOS will also systematically affect the critical point location. Clearly, it would be preferable to determine the critical properties directly from the simulation data without recourse to an EOS model. One approach starts by choosing a number of isotherms *within* the coexistence region close to the critical point. For a sufficiently large number of state points on each isotherm, a Maxwell construction can be carried out directly on the (P, v) data to obtain the apex of the coexistence curve from which P_c^* and v_c^* can be determined. As the coexistence curve is rather flat close to the critical point, a direct estimate of v_c^* will be of poor precision. By appealing to the empirical law of rectilinear diameters [13], however, v_c^* should lie, to a very good approximation, at the intersection of the coexistence curve and an extrapolated straight line bisector of tie-lines between orthobaric densities.

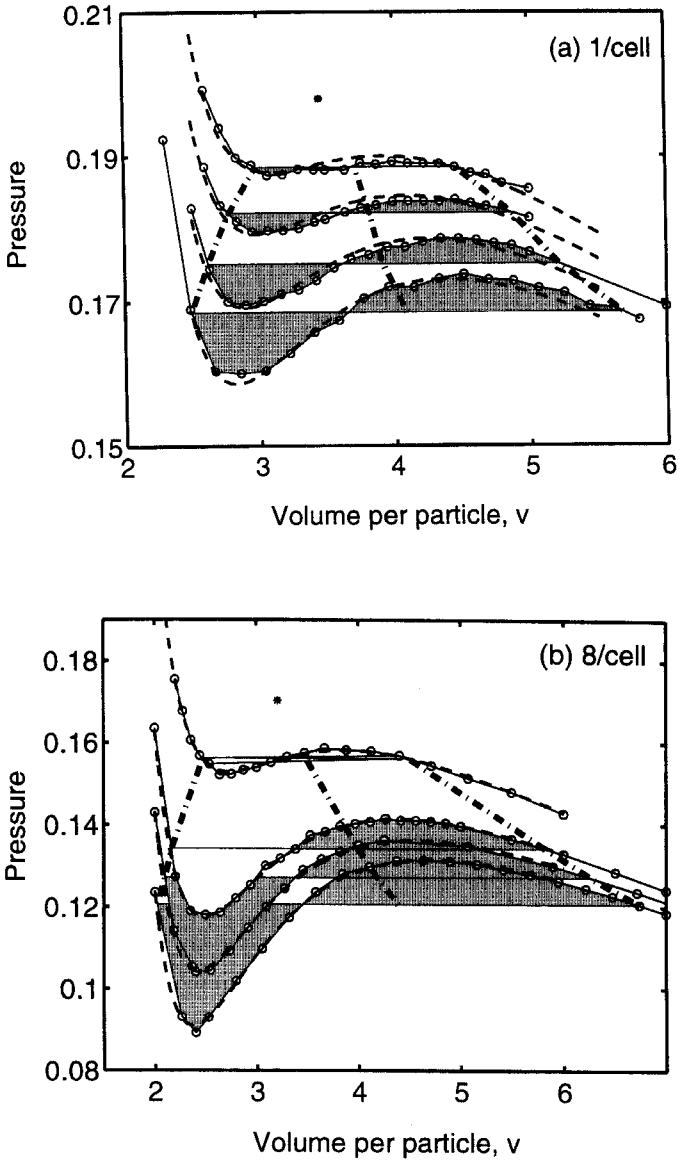

FIGURE 5 The coexistence region of the phase diagram, in the pressure-volume projection, for a cell constrained Lennard-Jones (12–6) fluid. Open circles denote raw simulation data while linear interpolation is performed to aid the Maxwell construction indicated by the shaded areas. The coexistence envelope and the rectilinear diameter are shown as bold dashed-dotted lines. Isotherms fitted by the HS-B_2-C equation of state model are also included (– – –) and the corresponding critical point is identified (*). (a) Single particle occupancy per cell with isotherms $T^* = 1.6724$, 1.6896, 1.7069 and 1.7220. (b) Eight particle occupancy per cell with isotherms $T^* = 1.3414$, 1.3560, 1.3710 and 1.4150.

TABLE IV Critical parameters for the isotherms of Figure 5

EOS	*n*	*a*	*b*	*c*	*g*	P_c^*	v_c^*	T_c^*	Z_c^*
HS-B_2-C	1	6.353	1.254	−0.0653	−0.154	0.198	3.454	1.742	0.393
HS-B_2-C	8	6.386	1.092	0.862	−0.0342	0.170	3.207	1.441	0.379

This method is demonstrated in Figure 5 both for the case of single particle cell occupancy with the isotherms at $T^* = 1.6724$, 1.6896, 1.7069 and 1.7220, as well as the corresponding results for 8 particle cell occupancy on the isotherms $T^* = 1.3414$, 1.3560, 1.3710 and 1.4150. In these simulations, the cutoff radius is set to $r_c = 4.00\sigma$. Unfortunately, even under the strictest constraint of single particle cell occupancy, convergence is slow very close to the critical point and, at the same time, accurate Maxwell construction becomes more difficult as the areas above and below the isotherm are both small.

Critical point determination using only simulation data remains inaccurate. After having built up a rather detailed picture of the coexistence region immediately below the T_c, however, an EOS model can now be fitted to the data with some confidence. In Figure 5, the HS-B_2-C EOS has been fitted to the four isotherms, with satisfyingly good agreement, as indicated by thin dashed lines. For both cell occupancy cases, the predicted critical points, shown as a star in Figure 5 and quoted in Table IV, lie close to an imagined intersection of the dashed-dotted lines in accordance with the law of rectilinear diameters.

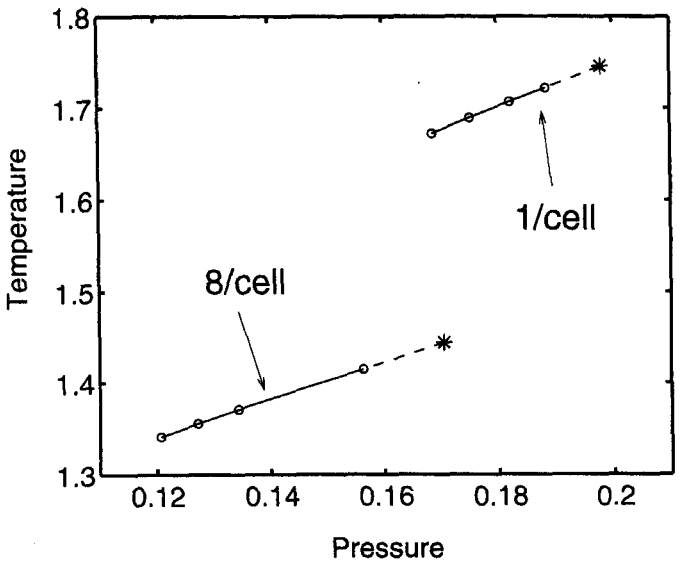

FIGURE 6 The vapor pressure curve in the temperature–pressure projection of the phase diagram for a cell constrained Lennard-Jones (12–6) fluid. Raw data from single particle and 8 particle cell occupancy simulations are indicated (○) corresponding to the isotherms of Figure 5. The straight line of best fit is extrapolated to the critical point (*) determined from the HS-B_2-C equation of state model and listed in Table IV.

In a (T, P) projection (Fig. 6), the pure simple fluid vapor pressure curve is very closely approximated by a straight line. Extrapolating the temperature to P_c^* of Table IV, yields $T_c^* = 1.746$ and $T_c^* = 1.444$ for single particle and 8 particle cell occupancy, respectively. With this combination of raw data anaylsis and EOS modelling, we believe that the results summarised in Table IV are close to the true critical parameters for each of these systems.

ANALYSIS OF VAN DER WAALS LOOPS IN SIMULATIONS

As verified above, the imposition of uniform single phase configurations by cell constraints will give rise to classical loops in the (P, v) isotherms. What happens to these loops as the constraint is relaxed by expanding the cell size and the number of particles per cell at fixed overall density? This question may as well be asked with respect to the normal periodic boundary condition simulations where the simulation boxes and occupation numbers are larger but still finite. In a recent series of articles, Nakanishi and coworkers [5] have described studies of the van der Waals loop in MC and MD simulations carried out for fluids with truncated and shifted Lennard-Jones potentials, thereby avoiding the need for long range correction of the type used here. It is claimed that the approximation $g(r) \simeq 1$ for $r > r_c$ enhances the unphysical loop which is related to the system size and to the magnitude of the gas–liquid surface tension. Evidence is produced showing that the loop, which is very prominent for simulations with 256 active particles, is nearly eliminated for 55296 particles. This observation is interpreted in terms of bubble formation at reduced pressure and the inability of small systems to develop large and long ranged density fluctuations under the normal simulation procedure with periodic boundary conditions.

The purpose here is to use the cell-constrained fluid models and the GvdW density functional formalism to interpret the van der Waals loops and further clarify the underlying mechanisms. This endeavour can be motivated on the strength of the fact that cell constraints and the corresponding configurational restrictions in the GvdW analysis permit estimation of the relative stability of density fluctuations. Thus, the cell constrained fluid model with 1 or 8 particles per cell of the same size accounts for a class of configurations which together will define what we mean by a "uniform fluid". A nonuniform fluid, on the other hand, can then be created by allowing the cell size to vary spatially in some systematic way. For example, a two-phase structure can be artificially created where a liquid

drop is represented by a cluster of small cells, in the center of the global simulation box, which is surrounded by a lattice of larger cells. Given the free energy corresponding to both the uniform $F^{(1)}$ and two-phase $F^{(2)}$ structures, then the density fluctuations within the coexistence curve of the bulk fluid can be accounted for by writing the approximate total partition function as,

$$Q \approx \exp(-\beta F^{(1)}) + \exp(-\beta F^{(2)}), \tag{11}$$

where $\beta = 1/(k_B T)$ as usual. Unfortunately, free energies are notoriously difficult to obtain from simulations. By focusing on qualitative mechanisms rather than quantitative analysis, however, the GvdW theory can, albeit with some loss in accuracy, provide the relevant free energies required. In its simplest form, denoted GvdW(S), the GvdW configurational free energy functional is,

$$F_c = k_B T \int_V d\mathbf{r}\, n(\mathbf{r}) \ln\left(\frac{n(\mathbf{r})}{1 - \bar{n}(\mathbf{r})\sigma^3}\right) + \frac{1}{2}\int d\mathbf{r} \int d\mathbf{r}' n(\mathbf{r}) n(\mathbf{r}') \phi_s(|\mathbf{r} - \mathbf{r}'|), \tag{12}$$

where $\phi_s(r)$ is the soft attractive part of the Lennard-Jones pair-potential,

$$\phi_s(r) = \begin{cases} 4\varepsilon\left((\sigma/r)^{12} - (\sigma/r)^6\right); & r > \sigma \\ 0; & \text{otherwise,} \end{cases} \tag{13}$$

and $\bar{n}$ is a coarse-grained particle density which delocalises microscopic position information over a characteristic volume. Details of the theory have been given elsewhere [14] and are not required here, except to note that it is consistent with a cell constrained fluid model and it yields free energies of quite good accuracy for both bulk fluids and gas–liquid interfaces. In particular, by setting $n = \bar{n}$ nonlocal entropy effects are neglected and the surface tension can be obtained analytically when the gas–liquid density distribution through a planar interface is assumed to take stepfunction form,

$$n(z) = \begin{cases} n_l; & z < 0 \\ n_g; & z \geq 0, \end{cases} \tag{14}$$

where n_l and n_g are the liquid and gas number densities, respectively. Specifically, the following expression for the surface tension γ is obtained,

$$\gamma_{sf} = \frac{3}{4}\pi\varepsilon\sigma^4(n_l - n_g)^2. \tag{15}$$

The true surface tension is smaller owing to spatial relaxation of the density profile and, to a lesser extent, the nonlocal entropy associated with excluded volume effects. Both these contributions can be estimated quite accurately by a more sophisticated GvdW calculation that incorporates both these mechanisms. For the present purposes, however, an empirical fit based on the so-called parachor parameter P_0 of Macleod and Sugden [15] will be adequate,

$$\gamma = P_0(n_l - n_g)^4. \tag{16}$$

To arrive at a simple expression for γ, note that the density profile is quite sharply defined at the triple point and $(n_l - n_g) \simeq \sigma^{-3}$, so that,

$$P_0(n_l - n_g)^4 \simeq \gamma_{sf} = \frac{3}{4}\pi\varepsilon\sigma^4(n_l - n_g)^2. \tag{17}$$

Thus, we obtain the parachor,

$$P_0 \simeq \frac{3}{4}\pi\varepsilon\sigma^{10}, \tag{18}$$

and, consequently, the surface tension.

$$\gamma \simeq \frac{3\pi\varepsilon}{4\sigma^2}\left((n_l - n_g)\sigma^3\right)^4, \tag{19}$$

which agrees favorably with experimental values for argon as illustrated in Figure 7. Armed with this simple analytical expression (19) for the surface tension of a Lennard-Jones gas–liquid interface we now proceed to consider the free energy of a two-phase structure composed of a central sphere of the phase of smallest volume surrounded in the simulation box by the phase of maximal volume, both phases being in coexistence at their equilibrium densities n_l or n_g, respectively.

Basic thermodynamic arguments [16] yield,

$$F^{(2)} = N_l f(n_l) + N_g f(n_g) + 4\pi r_s^2 \gamma, \tag{20}$$

where N_l and N_g are the particle numbers in each phase with the corresponding intensive total bulk Helmholtz free energy per particle f, given in the GvdW(S) theory by,

$$f(n) = k_B T\left(3\ln\lambda + \ln\left(\frac{n}{1 - n\sigma^3}\right)\right) - an, \tag{21}$$

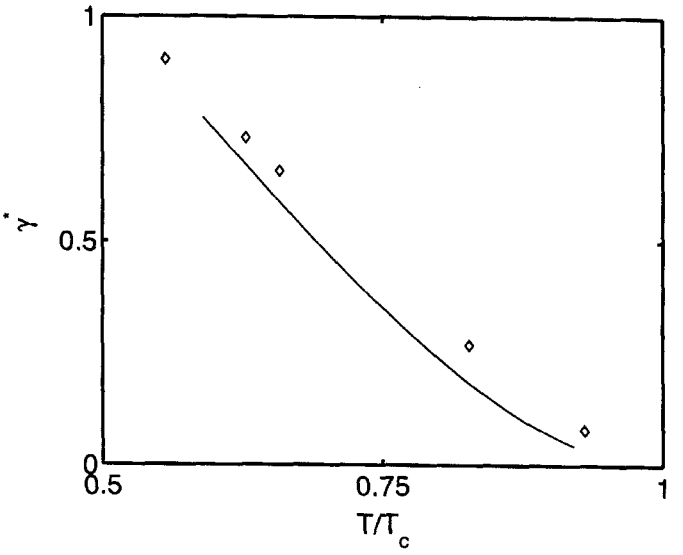

FIGURE 7 The reduced surface tension γ^* (*i.e.*, in Lennard-Jones units, $\varepsilon = \sigma = 1$) predicted by GvdW theory (Eq. (19)), and indicated by the solid line, is compared with experimental results [20] for argon ($\diamond$) reduced by best-fit LJ potential parameters as in Table III.

with the binding energy parameter,

$$a = -\frac{1}{2}\int d\mathbf{r}\, \phi_s(|\mathbf{r}|), \tag{22}$$

and the thermal wavelength,

$$\lambda = \frac{h}{\sqrt{2\pi m k_B T}}, \tag{23}$$

for particles of mass m. The last term of Eq. (20) is the surface free energy of a spherical drop or bubble with radius r_s given by,

$$r_s = \left(\frac{3}{4\pi} V_s\right)^{1/3}, \tag{24}$$

$$V_s = \min\left(\frac{N_l}{n_l}, \frac{N_g}{n_g}\right). \tag{25}$$

Similarly, the uniform fluid structure has a free energy,

$$F^{(1)} = Nf(n). \tag{26}$$

Now, compute the pressure inside the bulk coexistence curve as the appropriate derivative of Eq. (11) to obtain,

$$P = -k_B T \frac{\partial}{\partial V} \ln Q = \theta P^{(1)} + (1 - \theta) P^{(2)}, \tag{27}$$

where θ is the probability of finding the system in a single phase structure,

$$\theta = \frac{\exp(-\beta F^{(1)})}{\exp(-\beta F^{(1)}) + \exp(-\beta F^{(2)})}, \tag{28}$$

and $(1-\theta)$ is the complementary probability for the phase separated state. The corresponding pressures inherent to the two structures are,

$$P^{(1)} = \frac{k_B T n}{1 - n\sigma^3} - an^2, \tag{29}$$

$$P^{(2)} = P_{co} + \Delta P_s, \tag{30}$$

where P_{co} is the vapour pressure which would apply in the absence of surface tension,

$$P_{co} = P^{(1)}(n_l) = P^{(1)}(n_g), \tag{31}$$

and ΔP_s collects the surface tension contribution,

$$\Delta P_s = -\frac{\partial}{\partial V}(4\pi r_s^2 \gamma). \tag{32}$$

To resolve this derivative, first consider the case of a spherical liquid drop, with volume V_s, at the center of the global box, so,

$$V_s = \frac{4\pi r_s^3}{3} = \frac{N_l}{n_l} = \frac{N - n_g V}{n_l - n_g}, \tag{33}$$

$$r_s = \left(\frac{3(N - n_g V)}{4\pi(n_l - n_g)} \right)^{1/3}, \tag{34}$$

$$-\frac{\partial r_s}{\partial V} = \frac{n_g}{4\pi(n_l - n_g) r_s^2}, \tag{35}$$

whence it follows that,

$$\Delta P_s = \frac{2\gamma}{r_s} \left(\frac{n_g}{n_l - n_g} \right). \tag{36}$$

In the transposed case of a central spherical gas bubble, a similar argument leads to,

$$\Delta P_s = -\frac{2\gamma}{r_s}\left(\frac{n_l}{n_l - n_g}\right). \tag{37}$$

It is immediately clear that r_s scales with system size as $N^{1/3}$. Thus, the deviation of the two-phase pressure from its limiting value P_{co}, at fixed particle density n, is slowly diminishing with increasing system size. The extra free energy of the uniform phase grows like N, while that of the two-phase structure rises only as $N^{2/3}$ with system size. As N increases, therefore, at fixed average density n, the most probable configurations shift from uniform to two-phase structures. The overall effect is to diminish the loop with increasing system size. This is confirmed in Figure 8 where subcritical

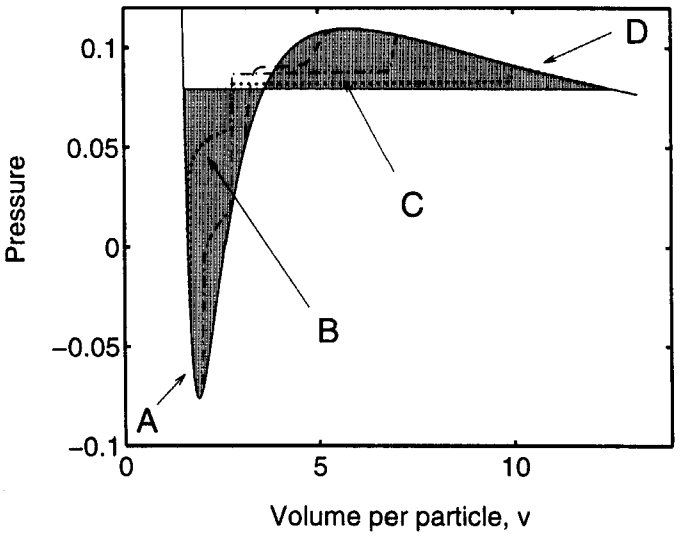

FIGURE 8 Subcritical ($T^* = 0.8T_c^*$) van der Waals loops calculated from GvdW theory are plotted for a uniform fluid and a spherical drop or bubble at gas–liquid coexistence. For the two-phase system, finite size effects are demonstrated by varying the total particle number N and the corresponding isotherms identified by line type as follows: $N = 3^{10}$ (· · ·); $N = 3^7$ (– · –); $N = 3^6$ (– – –). Single phase regions are labelled A and D, while in region B a spherical liquid droplet is surrounded by vapor and, conversely, a spherical gas bubble is surrounded by liquid in region C. Transitions between these states are observed, in most cases, to be very abrupt, giving rise to almost vertical lines. As N decreases, the isotherm must penetrate further into the coexistence region before drops or bubbles can be formed. The smooth solid line denotes the isotherm of a uniform fluid, that is the limiting response of arbitrarily small systems where density fluctuations are completely damped, and the shaded areas exhibit the corresponding Maxwell construction with the horizontal tie-line joining the coexistence densities.

isotherms calculated from Eq. (27) are compared for different N values and also with the uniform fluid limit.

The preceding argument is qualitative and simplified since the full ensemble of all fluctuations is not accounted for, merely those which are expected to dominate. Very crude approximations have also been committed to obtain the equation of state and the surface tension. Despite the doubtless poor accuracy of the finite system isotherms shown in Figure 8, they transparently illustrate the dominant underlying mechanism of loop reduction for increasing system size which will also be evident in simulation studies. No distinction is drawn here between simulations imposing periodic boundary conditions outside the global box (as in the standard algorithms) and those where cell constraints are applied. Particles continue to interact across cell boundaries in the latter, and are not subject to periodic replication except at distances greater than neighboring cells.

DISCUSSION AND CONCLUSION

The results above confirm the proposition that the localised confinement of simple fluid particles "regularizes" equilibrium statistical mechanical simulations by conferring a dramatic improvement in the rate of convergence. This raises the possibility of routine simulation techniques for molecular fluids. At the same time, imposing a confining cell structure clearly alters the physical observables, particularly the phase diagram around the critical point. The present results imply that the critical properties may be altered by roughly 20% or 10% with cell occupancy constraints of 1 or 8 particles per cell, respectively. Such deviations are likely to be generic for a wide range of molecular fluids and can be estimated using the modern theory of critical phenomena [17]. It is also possible to probe these effects by further simulations which systematically vary the degree of confinement of the fluid particles.

What is gained by cell-confinement? Most practically, a comparatively rapid convergence rate for ensemble averages at all state points. Furthermore, there is scope to implement routine simulations for simple and molecular fluids to obtain equations of state, conforming to standard empirical types, which display van der Waals loops and must be treated by the Maxwell construction in the coexistence region of the phase diagram. A major difficulty encountered with the conventional global box simulation under periodic boundary conditions lies in the inability to predetermine the scale of fluctuations, at a given state point, which can give rise to poor

statistics or unpredictable convergence to metastable structures of unknown properties. As discussed by Nakanishi and coworkers [5], the van der Waals loops are present for all finite size systems in the coexistence region. They are difficult to converge and to interpret. The simple analysis given here illuminates quite clearly the underlying mechanism driving them and how, in principle, the loop amplitude depends on system size. It seems certain, however, that conventional simulations will encounter difficulties or fail to resolve such gross fluctuations as represented by the uniform and two-phase structures anticipated through this analysis. Much more work is needed to establish the timescales of such density fluctuations and the chain lengths required, in either MC or MD simulations, to achieve satisfactory convergence. Simple arguments from nucleation theory suggest that the uniform and two-phase structures are separated by a free energy barrier which inhibits optimal phase space sampling in both types of simulation method.

References

[1] Allen, M. P. and Tildesley, D. J., "*Computer Simulation of Liquids*" (Clarendon, Oxford, 1987).
[2] Frenkel, D. and Smit, B., "*Understanding Molecular Simulations – From Algorithms to Applications*" (Academic Press, Sari Diego, 1996).
[3] Debenedetti, P. G., "*Metastable Liquids – Concepts and Principles*" (Princeton University Press, Princeton, New Jersey, 1996).
[4] Stanley, H. E., "*Introduction to Phase Transitions and Critical Phenomena*" (Oxford University Press, Oxford, 1971); Ma, S.-K., "*Modern Theory of Critical Phenomena*" (W. A. Benjamin, Reading, 1976).
[5] Kido, A., Kitao, O. and Nakanishi, K. (1992). "Can the van der Waals loop vanish?" *Chem. Phys. Lett.*, **199**, 403; Yamamoto, R., Kitao, O. and Nakanishi, K. (1995). "Can the van der Waals loop vanish? II. Effect of domain size", *Mol. Phys.*, **84**, 757; Yamamoto, R., Tanaka, H., Nakanishi, K. and Zeng, X. C. (1994). "Can the van der Waals loop vanish? Effect of surface free energy", *Chem. Phys. Lett.*, **231**, 401.
[6] van Kampen, N. G. (1964). "Condensation of a classical gas with long range attraction", *Phys. Rev. A*, **135**, 362.
[7] Abbas, S. and Nordholm, S. (1994). "Simple estimation of surface tension of single component fluids", *J. Colloid Int. Sci.*, **166**, 481.
[8] Clausius, R. (1881). "Über das Verhalten der Kohlensäure in Bezug auf Druck, Volumen und Temperatur", *Ann. Phys. Chem.*, **IX**, 337.
[9] Martin, J. J. (1979). "Cubic equations of state–which?", *Ind. Eng. Chem. Fundam.*, **18**, 81.
[10] Joffe, J. (1981). "Vapor-liquid equilibria with the Martin equation of state", *Ind. Eng. Clem. Process Des. Dev.*, **20**, 168.
[11] Kubic, W. L. (1982). "A modification of the Martin equation of state for calculating vapour-liquid equilibria", *Fluid Phase Equilibria*, **9**, 79.
[12] Press, W. H., Flannery, B. P., Teukolsky, S. A. and Vetterling, W. T., "*Numerical Recipes: The Art of Scientific Computing*" (Cambridge University Press, Cambridge, 1986).
[13] Rowlinson, J. S. and Swinton, F. L., "*Liquids and Liquid Mixtures*", 3rd edn. (Butterworth Scientific, London, 1982).
[14] Nordholm, S. and Haymet, A. D. J. (1980). "Generalized van der Waals theory. I. Basic formulation and application to uniform fluids", *Aust. J. Chem.*, **33**, 2013; Nordholm, S.,

Johnson, M. and Freasier, B. C. (1980). "Generalized van der Waals theory. III. The prediction of hard sphere structure", *Aust. J. Chem.*, **33**, 2139; Hooper, M. A. and Nordholm, S. (1984). "Generalized van der Waals theory. XIII. Curved interfaces in simple fluids", *J. Chem. Phys.*, **81**, 2432; Hooper, M. A. and Nordholm, S. (1987). "Generalized van der Waals analysis of critical drops and cavities", *J. Chem. Phys.*, **87**, 675; Freasier, B. C., Nordholm, S. and Woodward, C. E. (1989). "Generalized van der Waals theory of hard sphere oscillatory structure", *J. Chem. Phys.*, **90**, 5657.

[15] Reid, R. C., Prausnitz, J. M. and Poling, B. E., "*The Properties of Liquids and Gases*", 4th edn. (McGraw-Hill Inc., New York, 1987).

[16] Rowlinson, J. S. and Widom, B., "*Molecular Theory of Capillarity*" (Oxford University Press, Oxford, 1989).

[17] Lue, L. and Prausnitz, J. M. (1998). "Thermodynamics of fluid mixtures near to and far from the critical region", *AIChE J.*, **44**, 1455.

[18] Adams, D. J. (1975). "Grand canonical ensemble Monte Carlo for a Lennard-Jones fluid", *Mol. Phys.*, **29**, 307; "Calculating the low-temperature vapour line by Monte Carlo", *ibid*, **32**, 647 (1976); "Calculating the high-temperature vapour line by Monte Carlo", *ibid*, **37**, 211 (1979).

[19] Smit, B. (1992). "Phase diagrams of Lennard-Jones fluids", *J. Chem. Phys.*, **96**, 8639.

[20] Chapela, G. A., Saville, G., Thompson, S. M. and Rowlinson, J. S. (1977). "Computer simulation of a gas–liquid surface", *J. Chem. Soc., Faraday Trans. II*, **73**, 1133.